Thermal-Mechanical Response of Nearly Opaque Materials Exposed to Continuous Radiation

JOHN T. HOWE*
NASA Ames Research Center, Moffett Field, Calif.

A theoretical study of thermal stresses in a spherical shell exposed to an external uniform radiant and convective heating flux considers the effects of two mechanisms of energy transport in the material; absorption of radiant energy in depth and internal heat conduction. Stress distributions are obtained applicable to the initial transient heating prior to ablation, and the case of steady state ablation; showing the effects of geometry, transport properties, and ambient pressure. Conditions for internal and external spallation are derived. Simple expressions for thermal stresses are presented for special cases. The maximum thermal stress for ablating graphite-like materials are presented for incident radiant fluxes up to 250 kw/cm^2. An estimate of spall thickness is made. Some expressions for temperature profiles in materials are presented in the Appendix—including the case of a transient nonablating slab of finite thickness exposed to convective heating and nongray radiation (with arbitrary spectral detail); having internal conduction, internal spectral absorption and multiple internal reflections.

Nomenclature

a = inner radius of spherical shell
b = outer radius of spherical shell
c_p = specific heat of solid
E = modulus of elasticity of material
f = index in Eq. (A3)
$h_g(T_w)$ = enthalpy of gas at the wall temperature
$h(T_0)$ = enthalpy of solid before heating
Δh = enthalpy of sublimation per molecule
i = index in Eqs. (18) and (19)
k_c = thermal conductivity of material
k_ν = monochromatic linear absorption coefficient in material
k = Boltzmann constant
l = thickness of slab
m = defined by Eq. (26)
m_A = molecular weight
$\dot{m}$ = Langmuir sublimation rate
M = number of spectral bands
n = index in Eq. (2)
p = ambient pressure
p_0 = constant in Eq. (41)
p_{ve} = equilibrium vapor pressure
q_i = incident radiation flux
$q_{\nu i}$ = incident flux of frequency ν
q_ν = radiant flux at frequency band ν in material at the exposed surface
q_w = convective heating rate
r = radius
r_ν = spectral reflectivity within material
R_ν = external spectral reflectivity of exposed surface
t = time
T = temperature
v = surface recession rate
x = $(b_0 - r)$ defined in Fig. 1
X = subliming species [Eq. (46)]
y = $(b - r)$ defined in Fig. 1
α = coefficient of thermal expansion
β = defined by Eq. (12)
γ = defined by Eq. (20)
Γ = ratio of ultimate compressive strength to ultimate tensile strength in the circumferential direction
δ_r = depth of peak radial stress below exposed surface
δ_t = depth of penetration of ultimate circumferential compressive stress below exposed surface
Δ = shell thickness
ϵ = surface emissivity
K = sticking coefficient
μ = Poisson's ratio
ν = index in Eq. (1); spectral frequency band
ρ = density of material
σ = stress, also Stefan-Boltzmann constant

Subscripts

a = at the rear face
b = at the exposed face
c = conductivity
g = gas
i = incident
0 = conditions before heating
r = radial direction
t = tangential or circumferential direction
w = conditions at the wall

Received December 14, 1970; revision received June 21, 1971.
Index categories: Thermal Stresses; Radiation and Radiative Heat Transfer; Heat Conduction.
* Research Scientist.

Introduction

THE object of this study is to obtain approximate thermal stress predictions for materials exposed to heat fluxes up to hundreds of kilowatts per square centimeter and to assess the influence of geometry, transport phenomena, ambient conditions, and phase change on the stresses. Hopefully the results will provide insight for improving survivability for very high-speed entry into planetary atmospheres (the Jovian Planets in particular). Moreover, laboratory simulation of very high-speed entry will probably involve high power continuous wave laser facilities, and simple estimates of thermal effects may be useful in planning and interpreting experiments.

A number of analyses of elastic phenomena in semitransparent solids exposed to short pulse high power laser radiation have been presented over the past few years.[1-10] These include internal elastic explosions, implosions, and fracture; and the early formation of stress waves prior to the onset of ablation. These analyses are characterized by a time scale that is large enough that a temperature field can be defined in the material, but on the order of stress wave development time, and are formulated in terms of dynamic thermoelasticity theory. Penner and Sharma[5] define five characteristic

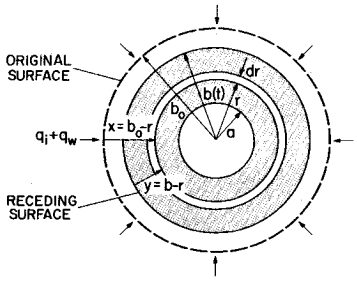

Fig. 1 Hollow sphere configuration.

times and provide the following estimates for "glassy" materials: temperature equilibration time ~sec, ablation time $\sim 10^{-1}$ sec, stress wave time $\sim 10^{-7}$ sec, temperature definition $\sim 10^{-14}$ sec, and energy deposition time 10^{-8} sec (for Q switched lasers).

With the advent of high power continuous wave lasers,[11] and their potential use in atmospheric entry simulation, we become interested in the longer time scales—after the initial stress waves, but prior to and during ablation. That is, we are concerned with times much larger than 10^{-7} in the Penner and Sharma ordering. This at once simplifies the problem in that static thermoelastic concepts can be employed (we neglect thermally induced structural vibration). In general, we are interested in the period of transient heating prior to ablation ($<10^{-1}$ sec) and in quasi-steady-state ablation (~sec).

Analysis

Consideration of a hollow sphere uniformly heated over the external surface allows simplification of the stress prediction because of symmetry, and still retains some of the features of interest from the entry viewpoint.

Energy Transfer

Figure 1 illustrates a hollow sphere exposed to uniform exterior convective heating q_w and incident radiative flux q_i of arbitrary spectral distribution. Before exposure, the material was at temperature T_0 and outer radius b_0, and subsequently is of instantaneous outer radius $b(t)$ as the exposed surface recedes at the rate $v(t)$ because of ablation.

Within the material, energy is transferred by conduction and radiation. The radiative flux just inside the exposed surface is

$$q_b(t) = \sum_{\nu=1}^{M} q_\nu(t) \tag{1}$$

where q_ν is the radiant energy flux in the frequency band ν of arbitrary bandwidth. At a depth y from the exposed face this flux has become $(b^2/r^2)q_\nu e^{-k_\nu y}$. At the inner face, $(b^2/a^2)r_{\nu a}q_\nu e^{-k_\nu(b-a)}$ is reflected back toward the exposed face, at which point the flux $r_{\nu b}r_{\nu a}q_\nu e^{-2k_\nu(b-a)}$ is reflected inward again and so on. That part of the flux not reflected at either surface is considered transmitted through the surface and lost from the system.

An energy balance on the element of thickness dr at radius r yields the differential equation

$$\frac{\partial T}{\partial t} = \frac{k_c}{\rho c_p}\frac{1}{r}\frac{\partial^2}{\partial r^2}(rT) + \frac{b^2}{r^2}\sum_{\nu=1}^{M}\frac{q_\nu}{\rho c_p}\times$$

$$\left\{(k_\nu)e^{k_\nu r}\sum_{n=0,2,4}^{\infty}(r_{\nu a}r_{\nu b})^{n/2}e^{-k_\nu[n(b-a)+b]} + \right.$$

$$\left.(k_\nu)e^{-k_\nu r}\sum_{n=1,3,5}^{\infty}r_{\nu a}(r_{\nu a}r_{\nu b})^{(n-1)/2}e^{-k_\nu[(n+1)(b-a)-b]}\right\} \tag{2}$$

where

$$b(t) = b_0 - \int_0^t v(t)dt \tag{3}$$

The first summation in Eq. (2) is over all M spectral bands, the last corresponds to rear face reflections, and the middle accounts for internal front face reflections.

Solutions of the one-dimensional slab form of Eq. (2) subject to convective and radiative heating are presented in the Appendix. The resulting expressions are far too awkward for present purposes, so we simplify the problem as follows. The one-dimensional slab approximation given by Eq. (A1) can be used if we limit our consideration to

$$k_\nu a \gg 2a/r \tag{4}$$

which means that the optical path length is much less than r.

Moreover, we will only be concerned with the absorption of the incident beam and disregard internal reflections, so that a restraint is imposed on the thickness $(b-a)$ to assure effective absorption of the radiant energy, i.e., be nearly opaque. That is

$$a^2q_\nu(a)/b^2q_\nu(b) = e^{-k_\nu(b-a)} \ll 1 \tag{5}$$†

which requires that

$$b/a \geq 1 + 2.3/k_\nu a \tag{6}$$

For effective retardation of heat transmission by conduction, relationship (6) applies with k_ν replaced by $\rho v c_p/k_c$. The energy Eq. (2) thus becomes

$$\frac{\partial T}{\partial t} = \frac{k_c}{\rho c_p}\frac{1}{r}\frac{\partial^2}{\partial r^2}(rT) + \sum_{\nu=1}^{M}\frac{q_\nu(t)k_\nu e^{-k_\nu(b-r)}}{\rho c_p} \tag{7}$$

Transient heating

For early time, before ablation begins, $v = 0$, and $b - r$ is x in Fig. 1. Further simplification is achieved by neglect of conduction, which is reasonable for times much less than the "conduction time"[12]

$$t \ll \rho c_p/k_c k_\nu^2 \tag{8}$$

at all wavelengths, which actually corresponds to a conduction flux much less than the radiative flux.

For a material heated only by internal absorption of radiation, Eq. (7) integrates to

$$T(x,t) = T_0 + \sum_{\nu=1}^{M}\frac{k_\nu}{\rho c_p}e^{-k_\nu x}\int_0^t q_\nu(t)dt \tag{9}$$

In the absence of ablation, the incident radiative flux is

$$q_i(t) = \sum_{\nu=1}^{M}\frac{q_\nu(t)}{(1-R_\nu)} \tag{10}$$

where R_ν is the reflectivity of the front face in the frequency band ν.

Steady-state ablation

If the one-dimensional slab approximation is made for heat transfer by internal conduction, Eq. (7) can be replaced by Eq. (A9). For the steady state, q_ν and v are approximately constant, $b-r = x-vt = y$, and Eq. (A9) can be transformed to coordinates fixed on the receding surface [Eq. (A10)] and integrated to obtain

$$T(y) - T_0 = (T_w - T_0)e^{-\beta k_\nu y} + \sum_{\nu=1}^{M}\frac{q_\nu e^{-k_\nu y}}{k_\nu k_c(\beta-1)}(1 - e^{-k_\nu y(\beta-1)}) \tag{11}$$

† The notation $q_\nu(a)$ refers to the radiative flux in the material at the inner face, and is used here only.

where T_0 is the temperature of the unheated material far from the exposed surface and

$$\beta = \rho v c_p / k_c k_\nu \tag{12}$$

A special case affords simplification: the radiation is absorbed at the surface ($k_\nu \to \infty$) and energy is conducted inward so that the temperature profile becomes

$$[T(y) - T_0]/[T_w - T_0] = \exp(-\rho v c_p y / k_c) \tag{13}$$

Another special case leads to the same form. That is a nonconducting material in which radiation is absorbed both at the surface and internally so that the temperature profile is

$$T(y) - T_0 = \sum_{\substack{\text{internally} \\ \text{absorbed bands}}} (q_\nu / \rho v c_p) e^{-k_\nu y} \tag{14}$$

For monochromatic internal radiation

$$(T(y) - T_0)/(T_w - T_0) = e^{-k_\nu y} \tag{15}$$

which is the same form as Eq. (13). For this "pure radiation" case, the required energy for the phase change is obtained by surface absorption of one or more bands of the incident radiative flux in the absence of internal conduction. The temperature profile for either special case [Eq. (13) or (15)] is shown in Fig. 2 where k_i is either $\rho v c_p / k_c$ or k_ν, respectively. Incidentally, the same profile also corresponds to the transient case before internal conduction or ablation are important as can be shown by Eq. (9) specialized to monochromatic radiation. This profile will be used later to typify all three special cases, whereas profiles corresponding to Eq. (11) will be generated for the more general case of energy transfer by combined internal absorption and conduction.

Thermal Stress

General

Because of symmetry, the only nonzero stress components due to thermal effects in the hollow sphere are the radial and circumferential tension (or compression) given by[13]

$$\sigma_r = \frac{2\alpha E}{(1-\mu)} \left[\frac{(r^3 - a^3)}{r^3(b^3 - a^3)} \int_a^b (T - T_0) r^2 dr - \frac{1}{r^3} \int_a^r (T - T_0) r^2 dr \right] \tag{16}$$

and

$$\sigma_t = \frac{2\alpha E}{(1-\mu)} \left[\frac{(2r^3 + a^3)}{2r^3(b^3 - a^3)} \int_a^b (T - T_0) r^2 dr + \frac{1}{2r^3} \int_a^r (T - T_0) r^2 dr - \frac{(T - T_0)}{2} \right] \tag{17}$$

Integration of Eqs. (16) and (17) for the temperature profile of Eq. (11) with $M = 1$ (monochromatic radiation) yields the thermal stresses

$$\sigma_r = \frac{2\alpha E}{(1-\mu)} \sum_{i=1}^{2} \frac{\gamma_i}{k_i^3 r^3} \left[\frac{(r^3 - a^3)}{(b^3 - a^3)} (k_i^2 b^2 - 2k_i b + 2) + \frac{(b^3 - r^3)}{(b^3 - a^3)} e^{-k_i(b-a)} (k_i^2 a^2 - 2k_i a + 2) - e^{-k_i(b-r)} (k_i^2 r^2 - 2k_i r + 2) \right] \tag{18}$$

and

$$\sigma_t = \frac{\alpha E}{(1-\mu)} \sum_{i=1}^{2} \frac{\gamma_i}{k_i^3 r^3} \left[\frac{(2r^3 + a^3)}{(b^3 - a^3)} (k_i^2 b^2 - 2k_i b + 2) - \frac{(2r^3 + b^3)}{(b^3 - a^3)} e^{-k_i(b-a)} (k_i^2 a^2 - 2k_i a + 2) + e^{-k_i(b-r)} (k_i^2 r^2 - 2k_i r + 2) - k_i^3 r^3 e^{-k_i(b-r)} \right] \tag{19}$$

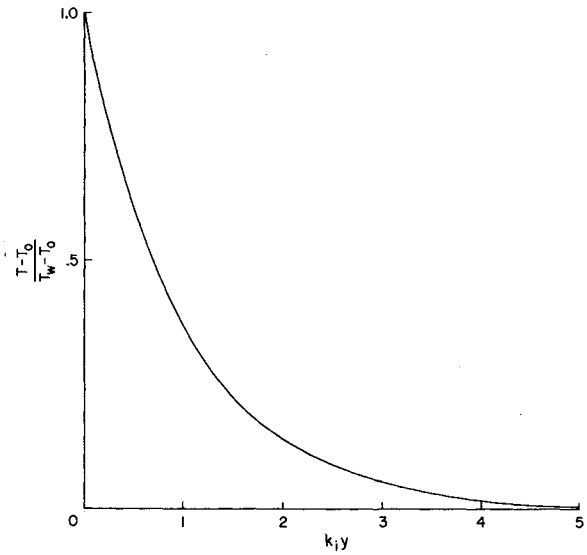

Fig. 2 Temperature profile for three special cases.

where

$$\gamma_1 = q_\nu/(\rho v c_p - k_\nu k_c),\ k_1 = k_\nu$$
$$\gamma_2 = [(T_w - T_0) - \gamma_1],\ k_2 = \rho v c_p / k_c \tag{20}$$

Special cases

For the special cases mentioned previously corresponding to the temperature profile of Fig. 2 the stresses become

$$\sigma_2 = \frac{2\alpha E}{(1-\mu)} \frac{(T_w - T_0)}{k_i^3 r^3} \left[\frac{(r^3 - a^3)}{(b^3 - a^3)} (k_i^2 b^2 - 2k_i b + 2) - e^{-k_i(b-r)} (k_i^2 r^2 - 2k_i r + 2) + e^{-k_i(b-a)} \times \frac{(b^3 - r^3)}{(b^3 - a^3)} (k_i^2 a^2 - 2k_i a + 2) \right] \tag{21}$$

and

$$\sigma_t = \frac{\alpha E}{(1-\mu)} \frac{(T_w - T_0)}{k_i^3 r^3} \left[\frac{(2r^3 + a^3)}{(b^3 - a^3)} (k_i^2 b^2 - 2k_i b + 2) + e^{-k_i(b-r)} (-k_i^3 r^3 + k_i^2 r^2 - 2k_i r + 2) - e^{-k(b-a)} \frac{(2r^3 + b^3)}{(b^3 - a^3)} (k_i^2 a^2 - 2k_i a + 2) \right] \tag{22}$$

The radial stress σ_2 is required to vanish at $r = a$ and b for an "unloaded" hollow sphere. The tangential stress is a maximum at $r = b$ and is

$$\sigma_t(b) = \frac{\alpha E}{(1-\mu)} (T_w - T_0) \left\{ -1 + \left(\frac{3b^3}{b^3 - a^3} \right) \times \left(\frac{1}{k_i b} \right) \left[\left(1 - \frac{2}{k_i b} + \frac{2}{k_i^2 b^2} \right) - \left(\frac{a^2}{b^2} - \frac{2a}{k_i b^2} + \frac{2}{k_i^2 b^2} \right) e^{-k_i(b-a)} \right] \right\} \tag{23}$$

Simpler expressions apply under restricted conditions. By virtue of Eq. (6) $k_i(b - a) \geq 2.3$ and the last trinomial on the right can be neglected. Further, if $k_i b \gg 2$,

$$\sigma_t(b) = [\alpha E(T_w - T_0)/(1-\mu)][-1 + \{3b^3/(b^3 - a^3)\}/k_i b] \tag{24}$$

And for very large k_i

$$\sigma_t(b)(1-\mu)/\alpha E(T_w - T_0) = -1 \tag{25}$$

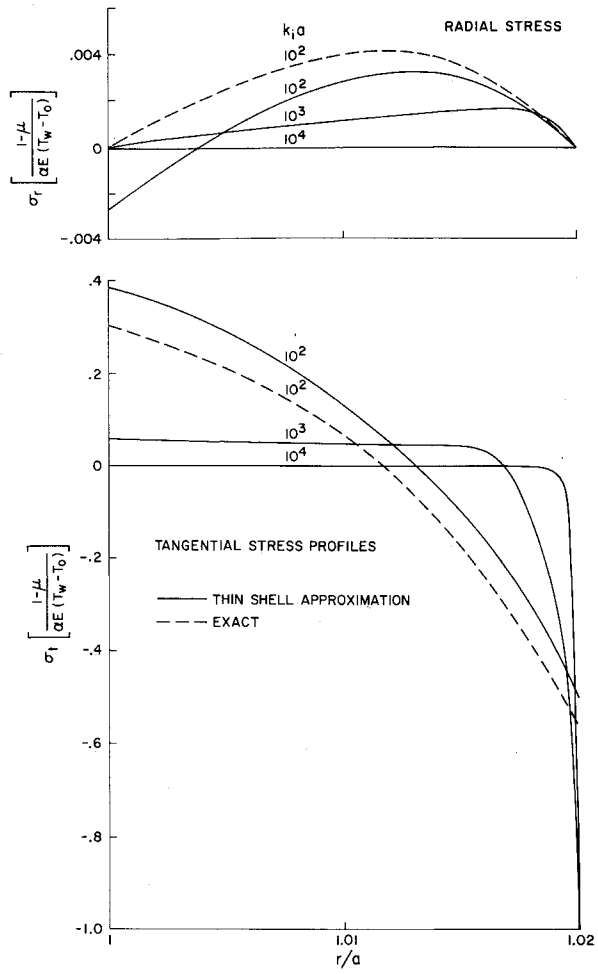

Fig. 3 Stress profiles; $b/a = 1.02$.

Thin shell approximation

For the special temperature profile of Fig. 2 let

$$b = a(1 + m) \tag{26}$$

where

$$m^2 \ll 1 \tag{27}$$

In accord with Eq. (6)

$$k_i a m = k_i \Delta \geq 2.3 \tag{28}$$

where Δ is the shell thickness. The thermal stress components Eqs. (21) and (22) become

$$\sigma_r = \frac{2\alpha E(T_w - T_0)}{(1-\mu)} \left[\left(1 - \frac{a^3}{r^3}\right)\left(\frac{1+m}{3k_i a m}\right) - \frac{1}{k_i a}\frac{a}{r} e^{-k_i a(1+m-r/a)}\right] \tag{29}$$

and

$$\sigma_t = \frac{\alpha E(T_w - T_0)}{(1-\mu)} \left[\left(2 + \frac{a^3}{r^3}\right)\left(\frac{1+m}{3k_i a m}\right) - e^{-k_\nu a(1+m-r/a)}\right] \tag{30}$$

The maximum radial stress σ_r occurs at

$$r/a = 1 + m - (1/k_i a)\ln(k_i a m/[1 - 2m]) \tag{31}$$

or at a depth of

$$\delta_r/a = (1/k_i a)\ln(k_i a m/[1 - 2m]) \tag{32}$$

below the exposed surface.

For very large $k_i a m$, the maximum normalized radial stress is

$$\bar{\sigma}_r \equiv \sigma_r(1-\mu)/\alpha E(T_w - T_0) = 2([1-m]/k_i a) \tag{33}$$

Similarly, the maximum circumferential stress occurs at $r = b$ (as shown below) and is

$$\bar{\sigma}_t(b) = [(1/k_i a m) - 1] \tag{34}$$

For large $k_i a m$, the limit of the normalized stress is thus

$$\bar{\sigma}_{t\max} = -1 \tag{35}$$

At the inner surface ($r = a$), the normalized tangential stress is

$$\bar{\sigma}_t(a) = [(1+m)/k_i a m - e^{-k_i a m}] \tag{36}$$

Within the constraints of Eqs. (27) and (28) the stress at a is tensile while that at b is compressive and

$$|\sigma_t(b)/\sigma_t(a)| > 1 \tag{37}$$

The first term in the parentheses of Eq. (36) dominates. Neglecting the last term and use of Eq. (34) leads to

$$\sigma_t(b)/\sigma_t(a) \approx (1 - k_i a m)/(1+m) \tag{38}$$

If the ratio of ultimate compressive to ultimate tensile strength in the circumferential direction is Γ, failure will occur on the front face if

$$(1 - k_i a m)/(1+m) > \Gamma \tag{39}$$

or otherwise on the rear face.

Application

Transient Heating

For early times before conduction is important, we consider the stresses associated with the temperature profile of Fig. 2 which are shown for a thin shell in Fig. 3. Normalized as they are, these stresses also correspond to two special steady ablation conditions mentioned previously: wherein radiation is absorbed entirely at the surface and heat is conducted inward and k_i is $\rho v c_p/k_c$; or where conduction is unimportant and one or more bands of radiation are absorbed at the surface-providing energy for the phase change, and one band of frequency ν is absorbed internally so that k_i is k_ν. The value $k_\nu a = 100$ violates the condition (28) slightly, and the corresponding result without the thin shell approximation is shown by the dashed curves. For a high value of $k_i a$ (strong absorption

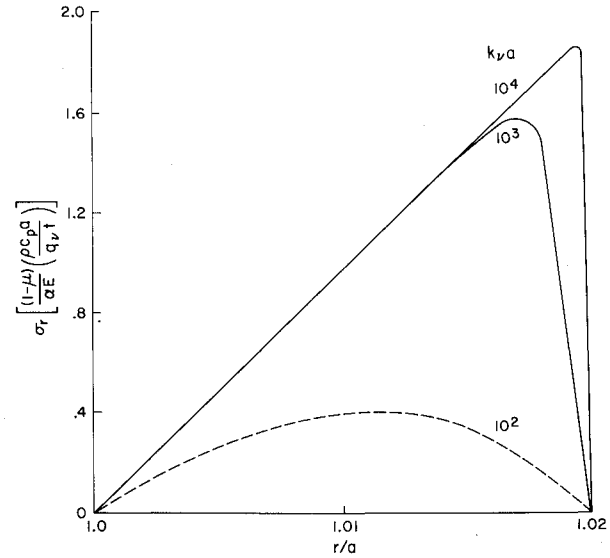

Fig. 4 Transient radial stress profiles; thin shell approximation, $m = 0.02$.

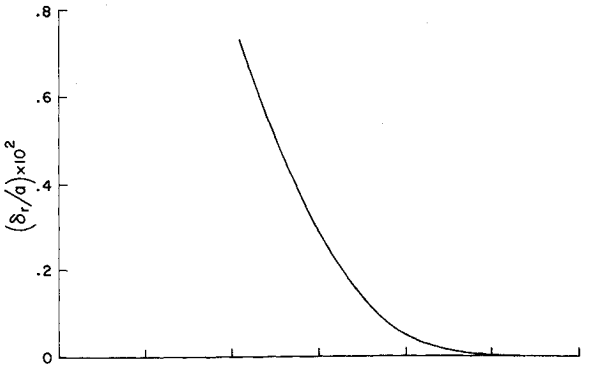

Fig. 5 Peak radial stress location; $m = 0.02$.

for $k_i = k_\nu$) the highly stressed region is near the exposed face, with the interior virtually unstressed.

The radial stress profile has been replotted in Fig. 4 renormalized by use of Eq. (9) with $x = 0$ to show a transient feature; that at a given instant, the radial stress is higher for stronger absorption and peaks closer to the exposed face $r = b$. The depth of the peak radial stress from the exposed surface is given by Eq. (32) and is shown in Fig. 5 while the magnitude of the peak radial stress is shown in Fig. 6.

During the initial exposure to a constant radiative flux, Eqs. (30) and (9) indicate that surface temperature and compressive circumferential thermal stress rise linearly with time. The shape of the ultimate compressive strength curve gives rise to the possibility of intermittent spallation of the exposed surface. That is, if the ultimate compressive strength rises with temperature and has positive curvative (e.g., Ref. 14), the surface could begin to spall and then stop before significant ablation begins as shown schematically in Fig. 7. Rhinehardt[15] may have observed such behavior experimentally.

Steady Ablation

The mass loss rate is needed for application of the thermal stress results. For simplicity, we consider the case of sublimation without heterogeneous or gas phase reactions. The modified Langmuir[16] sublimation rate is given by

$$\dot{m} = \rho v = K p_{ve}(m_A/2\pi k T_w)^{1/2}(1 - p/p_{ve}) \qquad (40)\ddagger$$

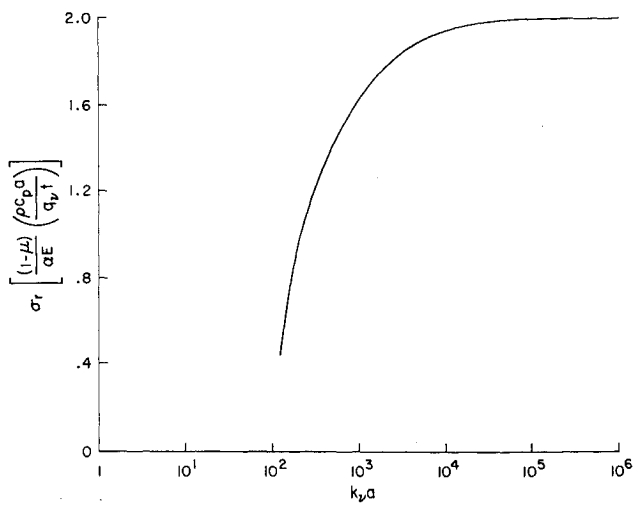

Fig. 6 Maximum radial stress; $m = 0.02$.

‡ A similar form is obtained if foreign gaseous species are present as shown by Ref. 17. Moreover, the case of chemical reactions is readily treated in a parallel manner, but requires a knowledge of reaction rate coefficients.

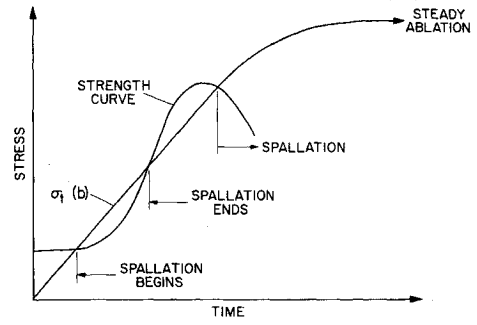

Fig. 7 Transient intermittent spallation.

where the equilibrium vapor pressure[18] is

$$p_{ve} = p_0 e^{-\Delta h/kT_w} \qquad (41)$$

according to Trouton's rule.

A normalized mass loss rate in a vacuum is defined by

$$\dot{m} \equiv (\dot{m}/Kp_0)(2\pi\Delta h/m_A)^{1/2} = (\Delta h/kT_w)^{1/2} e^{-\Delta h/kT_w} \qquad (42)$$

and is plotted in Fig. 8. The figure shows that the onset of significant sublimation occurs at $kT_w/\Delta h \approx 0.1$, which could be considered as an approximate sublimation temperature.

An energy balance extending deep into a material whose outer surface is exposed to convective heating and partially reflected spectral radiation—which is absorbed at the surface for some spectral bands and internally for others, yields

$$\sum_{\nu=1}^{M} q_{\nu i}(1 - R_\nu) = \rho v[h_g(T_w) - h_s(T_0)] + \epsilon\sigma T_w^4 - q_w \qquad (43)$$

An energy balance at the ablating surface yields

$$(k_c \partial T/\partial y)_w = - \sum_{\substack{\text{surface} \\ \text{absorbed bands}}} [q_{\nu i}(1 - R_\nu)] - q_w + \rho v[h_g(T_w) - h_s(T_w)] + \epsilon\sigma T_w^4 \qquad (44)$$

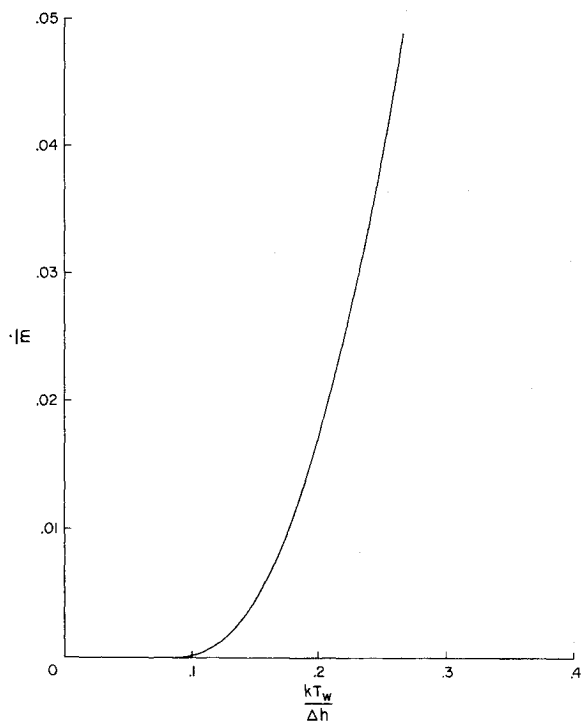

Fig. 8 Ablation rate.

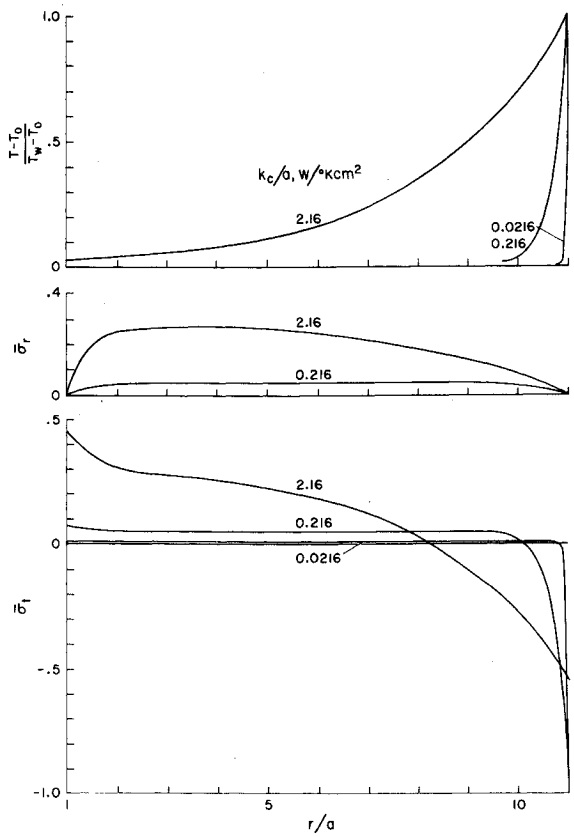

Fig. 9 Effect of conduction on stress; $k_\nu a = 10^5$, $T_w = 3600°K$, $p = 0$.

which combined with Eq. (43) gives

$$(k_c \partial T/\partial y)_w = \sum_{\substack{\text{internally} \\ \text{absorbed bands}}} [q_{\nu_i}(1 - R_\nu)] - \rho v c_p (T_w - T_0) \quad (45)$$

Equation (44) tell us that, in general, energy for the phase change at the surface can be provided by surface absorption, convection, and, if necessary, internal conduction so that the temperature gradient at the surface can be zero, positive or negative. But if there is neither surface absorption nor convection, then internal conduction, back to the subliming surface, of energy that had been absorbed internally, is the only mechanism for phase change and $(k_c \partial T/\partial y)_w > 0$; i.e., the peak temperature is internal.

On the other hand, Eq. (45) shows that surfaces subject to convective heating and/or surface absorption of radiation but with no internal absorption, $(k_c \partial T/\partial y)_w < 0$, and the peak temperature is at the surface.

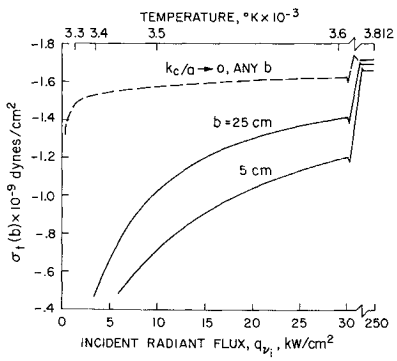

Fig. 10 Influence of outer radius and heat flux on tangential stress; $\Delta = 5$ cm, $p/p_{ve} = 0$, surface absorption.

To illustrate these features, we consider monochromatic radiation and will drop the spectral summation sign in the above relations. Equations (40, 43, 18, and 19) are to be solved for the unknowns ρv, q_{ν_i}, σ_r, and σ_t if T_w is specified; and q_ν is taken to be the left side of Eq. (43) with $M = 1$. If q_{ν_i} is specified, T_w is computed.

Moreover, the ablation model is simply

$$X(s) \to X(g) \quad (46)$$

and some properties akin to those of carbon suffice for illustrative purposes; elastic properties of carbon,[14] gas molecular weight of 30, and gas enthalpy about that of C_3 (Ref. 19) was employed; as was the vapor pressure of equilibrium carbon vapor over graphite obtained from Ref. 20 which matches the sublimation point of Ref. 21 and the triple point of Ref. 22. Surface emissivity is 0.8 and the reflectivity is zero.

Results of the computation for the Langmuir limit are presented in Fig. 9 for strong absorption ($k_\nu a = 10^5$) showing the effects of varying the thermal conductivity, k_c. The inner radius a also appears so that the curves are generally useful for ratios of k_c/a as shown. To illustrate, let a be 0.2 cm and the sphere wall be 2 cm thick. For this example the general temperature profiles [Eq. (11)] were employed and are shown at the top.

For the lowest value of $k_c/a = 0.0216$ w/°K cm², the high temperature region is close to the exposed surface with the result that the radial stress profile is essentially zero while the tangential stress is negligible in the interior but very high in the thin layer near the exposed face.

By way of contrast, for the high value of $k_c/a = 2.16$ w/°K cm² (corresponding approximately to graphite) the entire thickness of the shell is heated and the peak radial stress is almost as high as the tangential stress. Note that increased conductivity has reduced the compressive stress on the exposed face, but increased the tensile stress on the rear face. If the material were weaker in tension than in compression, failure would probably occur on the rear face rather than the exposed surface.

It may be noted that for this example where radiant energy is absorbed very close to the surface, energy is immediately available for the phase change, the temperature profiles are single valued, and the stresses could have been calculated with the simple temperature profiles of Fig. 2. Note that the maximum normalized compressive tangential stress is almost the limiting value -1 given by Eq. (25) for the special cases.

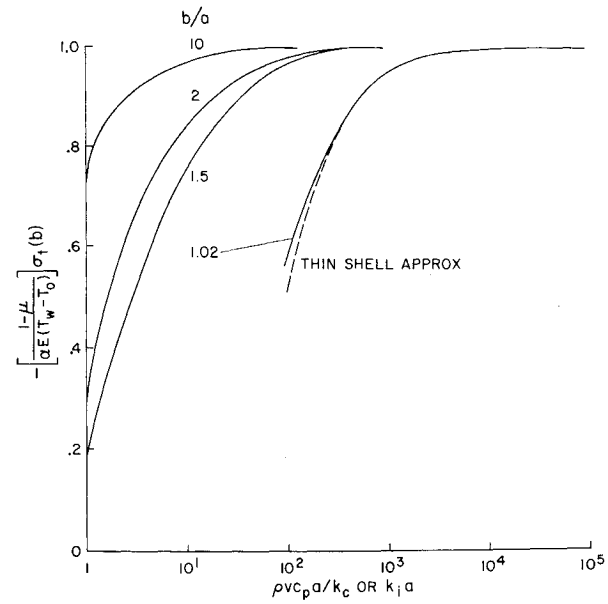

Fig. 11 Tangential stress on exposed face.

It will be seen subsequently that for deep penetration of radiation, the situation is altered significantly.

More generally, the influence of the incident radiant flux on the tangential stress at the exposed surface is shown in Fig. 10 for a sphere ablating in a vacuum. Absorption is essentially at the surface. The two solid curves are for a given heat shield thickness (5 cm) with different outer radii. For radiant fluxes up to about 30 kw/cm², the small radius has significantly lower stress than the larger radius, but the differences become unimportant at very high heating rates as shown by the figure. The thermal conductivity for both curves was $k_c = 0.432$ watt cm/cm² °K corresponding approximately to graphite. The upper dashed curve is the result if thermal conductivity is allowed to approach zero and represents an upper limit on the stresses. The difference between the dashed curve and the solid curves represents the stress reduction by internal conduction-very significant for low fluxes but unimportant for high flux. The upper limit on the stress is very sensitive to incident fluxes below about 2 kw/cm², but rises only 5% for fluxes between 30 and 250 kw/cm². It is essentially limited by the ablation temperature.

If we use the specialization for surface absorption and internal conduction, Eq. (23) gives the surface stress which is normalized and plotted in Fig. 11. As $k_c/a \to 0$, $\bar{\sigma}_t(b) \to -1$ for any b/a, which corresponds to the dashed curve in Fig. 10. For this case, high conductivity tends to reduce the surface stress. Incidentally, the same specialization applies to the case of surface absorption of one or more radiation bands and internal absorption of one band for negligible thermal conduction as noted previously in connection with Eq. (15), for which, the abscissa of Fig. 11 becomes $k_\nu a$. The significance of the figure is that a lower absorption coefficient (deeper penetration of radiation) reduces the peak tangential stress.

The influence of ambient pressure on the upper limit of the surface stress ($k_c/a \to 0$) is shown in Fig. 12. According to Eq. (40), the increased pressure reduces the ablation rate, so that for a given incident flux, the material ablates at a higher surface temperature [Eq. (43)] with a corresponding increase in stress. A reduction in vapor pressure (such as in Ref. 23) has a similar effect.

The effect of optical properties on thermal stress is shown in Fig. 13 for a fixed thermal conductivity. The upper set of curves shows that for strong absorption of radiation ($k_\nu a = 10^5$), the temperature profile is single valued of the type shown by Fig. 2. But for deeper penetration of radiation ($k_\nu a = 50$ or 20), there is an overshoot in temperature so that the peak temperature is internal rather than at the surface The reason is that the mechanism for ablation is therma

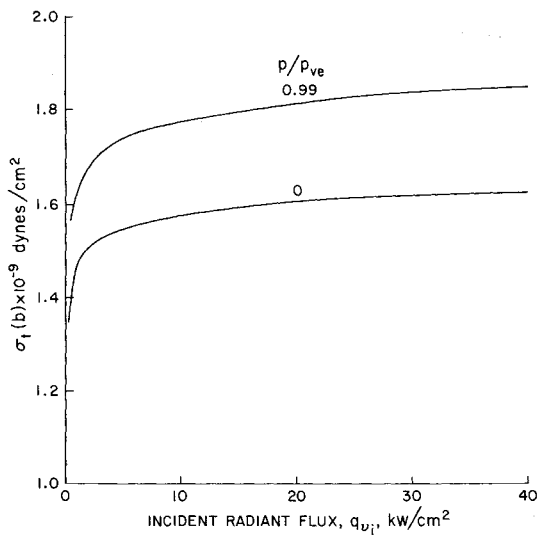

Fig. 12 Influence of pressure on surface stress; $k_c/a \to 0$, surface absorption.

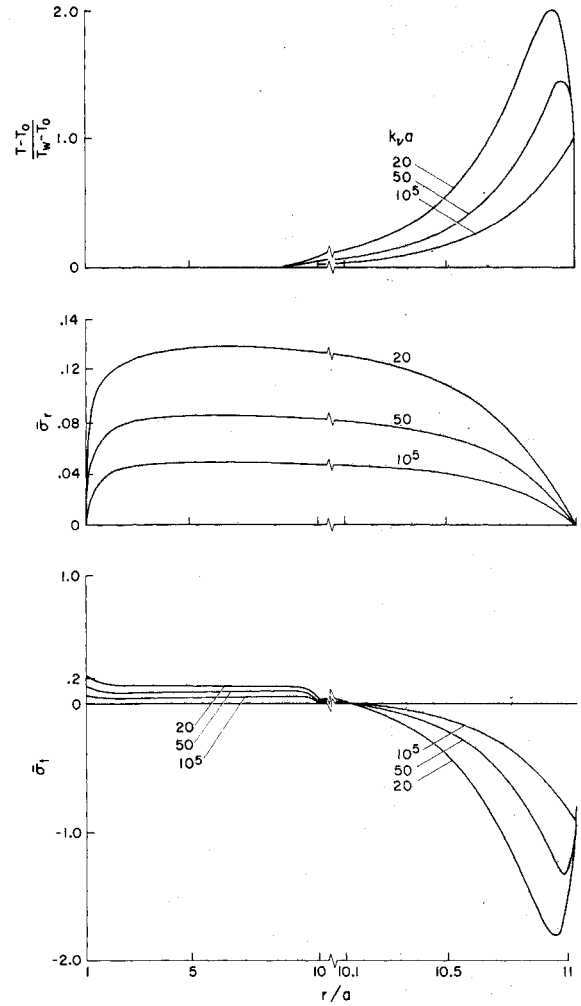

Fig. 13 Effect of optical properties on stress; no surface absorption or convection, $k_c/a = 0.216$, $T_w = 3600$°K, $p/p_{v_e} = 0$, $b/a = 11$.

energy conducted to the surface from the interior—which requires a temperature increasing inwardly.

It may be noted in Fig. 13 that the deeper penetration increases the radial stress σ_r internally, and the tangential stress σ_t in tension at $r = a$, and in compression near the exposed surface—corresponding to the temperature overshoot.

The extent of the overshoot in temperature and tangential stress is shown in the upper part of Fig. 14 as a function of the internal absorption coefficient. A buildup of gas pressure in the internal voids of the material may be expected (but was not included in the analysis) because of the high internal temperature. The internal equilibrium vapor pressure would exceed the compressive tangential stress for $(T - T_0)/(T_w - T_0)$ greater than about 1.3 (or $k_\nu a$ less than about 80).

Particles

Figures 10 and 12 showed that the tangential stresses exceed 10^9 dynes/cm² for incident fluxes of a few kw/cm² absorbed at the surface; and for low values of k_c/a, the stress is concentrated in a thin layer near the exposed surface (Fig. 9). If the surface stress exceeds the ultimate compressive strength of the material, one may expect thermomechanical failure at the surface. We could speculate that the thickness of the spalled material would not exceed the depth of material stressed at the ultimate strength. For $k_i b \gg 2$ and $e^{-k_i \Delta} \ll 1$, this depth is approximated by manipulating Eq. (22) and is

$$\delta_t = -\frac{1}{k_i} \ln \left[\frac{1}{k_i b} \frac{(2b^3/a^3 + 1)}{(b^3/a^3 - 1)} - \frac{(1 - \mu)\sigma_{t_{ult}}}{\alpha E (T_w - T_0)} \right] \quad (47)$$

for large $k_i b$ that is

$$\delta_t = -\frac{1}{k_i} \ln \left[-\frac{(1-\mu)\sigma_{t_{ult}}}{\alpha E (T_w - T_0)} \right] \tag{48}$$

where a negative number is to be substituted for $\sigma_{t_{ult}}$, and k_i is $\rho v c_p / k_c$. Of course if k_i is taken to be k_ν, the aforementioned applies to the other special case of surface absorption of part of the incoming radiation and internal absorption of one band where conduction is unimportant. In Eq. (48) the bracketed terms must be less than unity for spallation to occur because of Eq. (25) and $\sigma_t \geq \sigma_{t_{ult}}$ for spallation.

For illustrative purposes, suppose $T_w - T_0$ is between 3500°K and 3800°K for a material having the properties $\alpha = 3.6 \times 10^{-6}$ cm/cm °K, $E = 10^{11}$ dyne/cm^2, $\mu = 0.2$, ultimate compressive strength of 10^9 dyne/cm^2, $k_c = 0.45$ watt/cm °K and the vapor pressure of graphite; the spall thickness would be on the order of 1000 μ to 500 μ for $p/p_{ve} = 0$. For the special pure radiation case with negligible conduction but with $10^2 \leq k_\nu \leq 10^5$ cm^{-1}, the spall thickness estimate varies from about 50 to a twentieth of a micron.

For the more complicated general case of internal absorption with conduction supplying the energy for sublimation (Fig. 13), the peak stress moves inward about 80 μ for $k_\nu a = 50$ (where $a = 0.2$ cm) so that the highly stressed region is still thin—of the order of hundreds of microns.

Of course if failure occurs in the binder of graphitic materials, the resulting particles would be essentially grain size ($\sim$10 μm).

Spallation by thermal stresses will affect both the surface recession rate and the incoming radiative flux.

Summary and Conclusions

This study of the thermal stresses in an opaque spherical shell subject to uniform radiative and convective heating of the exterior surface included two mechanisms of energy transport within the material—heat conduction and internal absorption of radiation.

Three special cases were characterized by a single temperature profile-transient heating of a nonablating material by radiation for early time (before conduction is important), quasi-steady state heating of an ablating surface by radiation and convection with internal heat conduction but no internal radiation, and quasi-steady state heating of an ablating material by banded radiation wherein one band is absorbed internally and the remainder is absorbed at the surface. The more general case without special limitations was examined in detail.

Tangential stress tends to dominate. Where energy does not penetrate deeply into the material the stress is compressive and confined to a thin layer at the exposed surface. For deep penetration, the tangential stress on the inner face of the shell is tensile and can be significant. Failure could occur at either the exposed surface in compression or at the inner surface in tension depending on the relative compressive and tensile strength.

Internal conduction tends to relieve the peak stresses. Internal absorption of radiation tends to relieve the peak stress if the energy for phase change is supplied at the surface by convective heating or surface absorption; but tends to increase both the peak stress and peak temperature as well as shift them inward from the exposed surface if the energy for the phase change is supplied by internal conduction outward from radiation that had been absorbed in depth.

For graphite-like ablating materials exposed to monochromatic radiation, the peak compressive stress at the exposed face is a strong function of incident fluxes under 30 kw/cm^2, but a very weak function of higher fluxes out to 250 kw/cm^2. Both small outer radius and internal conduction effectively reduce the stress for the lower radiant fluxes, but are of little influence at the very high fluxes.

It is estimated that spalled particles will be small—perhaps grain size for graphitic materials. However, spallation can influence the surface recession rate and perhaps the flux incident on the surface by scattering and absorbing the radiation.

Results suggest that semitransparent materials with embedded reflecting sites may offer better thermal protection than high-temperature ablation for radiative environments—at least from thermal stress and mass removal considerations.

Appendix: Energy Transport—Slab Approximation

Transient Solutions

The differential equation for heat conduction and the absorption of incident spectral radiation in a slab of finite thickness including internal reflections is

$$\frac{\partial T}{\partial t} = \frac{k_c}{\rho c_p}\frac{\partial^2 T}{\partial x^2} + \sum_{\nu=1}^{M} \frac{q_\nu(t) k_\nu}{\rho c_p} \left[e^{-k_\nu y} \sum_{n=0,2,4,6}^{\infty} (r_{\nu a} r_{\nu b})^{n/2} \times e^{-nk_\nu \Delta} + r_{\nu a} e^{k_\nu y} \sum_{n=1,3,5}^{\infty} (r_{\nu a} r_{\nu b})^{(n-1)/2} e^{-(n+1)k_\nu \Delta} \right] \tag{A1}$$

where

$$y = x - \int_0^t v(t)dt \tag{A2}$$

and Δ is the instantaneous thickness of the slab. Equation (A1) is the slab equivalent to Eq. (2). The solution for a slab exposed to combined convective and constant spectral radiative heating with the rear surface insulated and partially reflecting and partially transmitting radiation is

$$\begin{aligned} T(x,t) - T_0 = {} & \left\{ \frac{q_w}{\rho c_p \Delta} + \sum_{\nu=1}^{M} \frac{q_\nu}{\rho c_p \Delta} \times \right. \\ & \left[r_{\nu a} \sum_{n=1,3,5}^{\infty} (r_{\nu a} r_{\nu b})^{(n-1)/2} e^{-(n+1)k_\nu \Delta} (e^{k_\nu \Delta} - 1) \right. \\ & \left. \left. - \sum_{n=0,2,4,6}^{\infty} (r_{\nu a} r_{\nu b})^{n/2} e^{-nk_\nu \Delta} (e^{-k_\nu \Delta} - 1) \right] \right\} \times \\ & \left(t + \frac{\rho c_p}{k_c}\frac{x^2}{2} - \frac{\rho c_p}{k_c} x\Delta \right) + \sum_{f=0}^{\infty} \frac{\Delta^2}{f^2\pi^2 k_c} \times \\ & \left\{ -q_w \left(\frac{\rho c_p}{k_c} \right)^{1/2} + \frac{2}{\Delta} \sum_{\nu=1}^{M} \frac{q_\nu k_\nu^2}{(k_\nu^2 + f^2\pi^2/\Delta^2)} \times \right. \\ & \left[r_{\nu a} \sum_{n=1,3,5}^{\infty} (r_{\nu a} r_{\nu b})^{(n-1)/2} e^{-(n+1)k_\nu \Delta} [1 - (-1)^f e^{k_\nu \Delta}] \right. \\ & \left. \left. - \sum_{n=0,2,4}^{\infty} (r_{\nu a} r_{\nu b})^{n/2} e^{-nk_\nu \Delta} (1 - (-1)^f e^{-k_\nu \Delta}) \right] \right\} \times \\ & \cos \frac{f\pi x}{\Delta} e^{-(f^2\pi^2 k_c t/\rho c_p \Delta^2)} + \sum_{\nu=1}^{M} \frac{q_\nu}{k_c} \left[r_{\nu a} \sum_{n=1,3,5}^{\infty} (r_{\nu a} r_{\nu b})^{(n-1)/2} \times \right. \\ & e^{-(n+1)k_\nu \Delta} \left(x e^{k_\nu \Delta} - \frac{1}{k_\nu} e^{k_\nu x} \right) - \sum_{n=0,2,4}^{\infty} (r_{\nu a} r_{\nu b})^{n/2} \times \\ & \left. e^{-nk_\nu \Delta} \left(x e^{-k_\nu \Delta} + \frac{1}{k_\nu} e^{-k_\nu x} \right) \right] \end{aligned} \tag{A3}$$

for early time before ablation begins. For monochromatic radiation the summation over ν spectral bands is dropped, and for no internal reflections, only the $n = 0$ term survives

§ This result corresponds loosely to Eq. (36) of Ref. 24; except that the latter is for a semi-infinite slab without internal reflections where radiative properties are averaged over the spectrum of the radiant source.

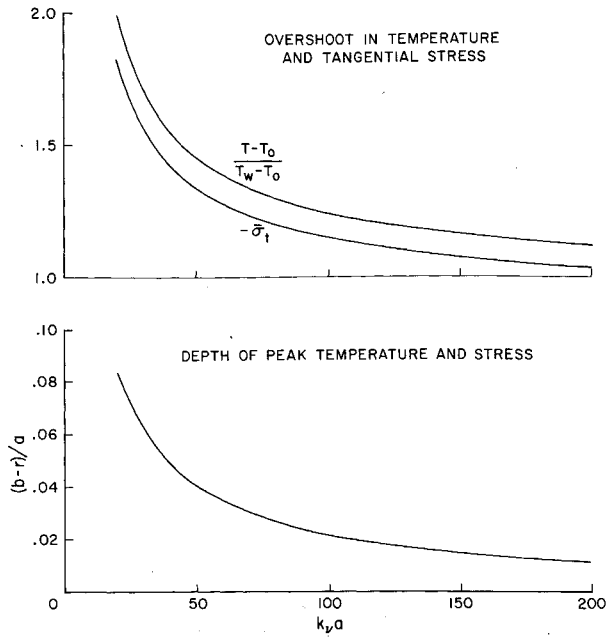

Fig. 14 Effect of internal absorption on peak temperature and stress; no surface absorption or convection, $k_c/a = 0.216$, $b/a = 11$, $T_w = 3600°K$, $p = 0$.

so that

$$T(x,t) - T_0 = \left[\frac{q_w}{\rho c_p \Delta} - (e^{-k_\nu \Delta} - 1)\right]^{\cdot} \times \left(t + \frac{\rho c_p}{k_c}\frac{x^2}{2} - \frac{\rho c_p}{k_c} x\Delta\right) + \sum_{f=0}^{\infty} \frac{\Delta^2}{f^2\pi^2 k_c} \times \left\{-q_w\left(\frac{\rho c_p}{k_c}\right)^{1/2} - \frac{2}{\Delta}\left[1 - (-1)^f e^{-k_\nu \Delta}\right]\right\} \times \cos\frac{f\pi x}{\Delta}\, e^{-(f^2\pi^2 k_c t/\rho c p \Delta^2)} - \frac{q_\nu}{k_c}\left(x e^{-k_\nu \Delta} + \frac{1}{k_\nu} e^{-k_\nu x}\right) \quad (A4)$$

The comparable result for a cold rear surface is

$$T(x,t) - T_0 = (q_w + q_\nu)\left(\frac{\Delta - x}{k_c}\right) - \sum_{=0}^{\infty} 2\left\{\frac{q_\nu}{k_\nu k_c} e^{-k_\nu \Delta}\left[\frac{1}{(f+\frac{1}{2})\pi} - \frac{(f+\frac{1}{2})\pi}{[k_\nu^2\Delta^2 + (f+\frac{1}{2})^2\pi^2]}\right] \times \sin\left(f+\frac{1}{2}\right)\pi - \frac{q_\nu \Delta}{k_c[k_\nu^2\Delta^2 + (f+\frac{1}{2})^2\pi^2]} + \frac{\Delta(q_w + q_\nu)}{(f+\frac{1}{2})^2\pi^2 k_c}\right\} \cos\left(f+\frac{1}{2}\right)\pi \frac{x}{\Delta} \exp\left[-\left(f+\frac{1}{2}\right)^2 \times \frac{\pi^2}{\Delta^2}\frac{k_c t}{\rho c_p}\right] + \frac{q_\nu}{k_c k_\nu}(e^{-k_\nu \Delta} - e^{-k_\nu x}) \quad (A5)$$

The special case of exposure to laser radiation only without internal reflections for early time where internal conduction is negligible is obtained by rewriting the differential Eq. (A1)

$$\partial T(x,t)/\partial t = [q_\nu(t) k_\nu/\rho c_p] e^{-k_\nu x} \quad (A6)$$

which can be integrated to obtain

$$[T(x,t) - T_0]/[T_w(t) - T_0] = e^{-k_\nu x} \quad (A7)$$

where

$$T_w(t) - T_0 = \frac{k_\nu}{\rho c_p}\int_0^t q_\nu(t)dt \quad (A8)$$

Steady Ablation Solutions

Here it is assumed that the slab is semi-infinite in extent, and internal reflections are neglected. The differential Eq. (A1) becomes

$$\frac{\partial T}{\partial t} = \frac{k_c}{\rho c_p}\frac{\partial^2 T}{\partial x^2} + \sum_{\nu=1}^{M} \frac{q_\nu(t) k_\nu}{\rho c_p} e^{-k_\nu y(x,t)} \quad (A9)$$

which allows arbitrary spectral detail. For steady ablation, this is transformed by use of Eq. (A2) with constant v to

$$\frac{d^2 T}{dy^2} + \frac{\rho v c_p}{k_c}\frac{dT}{dy} + \sum_{\nu=1}^{M} \frac{q_\nu k_\nu}{k_c} e^{-k_\nu y} = 0 \quad (A10)$$

The solution is readily found to be

$$T(y) - T_0 = (T_w - T_0)\exp\left[-\frac{\rho v c_p}{k_c} y\right] + \sum_{\nu=1}^{M} \frac{q_\nu}{(k_\nu k_c - \rho v c_p)}\left(\exp\left[-\frac{\rho v c_p}{k_c} y\right] - e^{-k_\nu y}\right) \quad (A11)$$

Both ρv and T_w are determined from two additional relationships; an energy balance which allows convective and radiative heating, and a relation between wall temperature and vapor pressure. Equation (A11) is similar to Eq. (22) of Ref. 24 except that the present result preserves the spectral detail.

References

[1] White, R. M., "Elastic Wave Generation by Electron Bombardment or Electromagnetic Wave Absorption," *Journal of Applied Physics*, Vol. 34, 1963, p. 2123.

[2] Carome, E F., Clard, N. A., and Moeller, C. E., "Generation of Acoustic Signals in Liquids by Ruby Laser Induced Thermal Stress Gradients," *Applied Physics Letters*, Vol. 4, No. 6, 1964, p. 95.

[3] Bullough, R. and Gilman, J. J., "Elastic Explosions in Solids Caused by Radiation," *Journal of Applied Physics*, Vol. 37, No. 6, 1966, p. 2283.

[4] Conners, G. H. and Thompson, R. A., "A Continuum Mechanical Model for Laser Induced Fracture in Transparent Media," *Journal of Applied Physics*, Vol. 37, No. 9, 1966, p. 3434.

[5] Penner, S. S. and Sharma, O. P., "Interaction of Laser Radiation With an Absorbing Semi-Infinite Solid Bar," *Journal of Applied Physics*, Vol. 37, No. 6, 1966, p. 2304.

[6] Morland, L. W., "Generation of Thermoelastic Stress Waves by Impulsive Electromagnetic Radiation," *AIAA Journal*, Vol. 6, 1968, pp. 1063–1066.

[7] Michaels, J. E., "Thermally Induced Elastic Wave Propogation in Slender Bars," *Proceedings of the Third U.S. National Congress of Applied Mechanics*, ASME, 1959, pp. 209–213.

[8] Gournay, L. S., "Conversion of Electromagnetic to Acoustic Energy by Surface Heating," *Journal of the Acoustical Society of America*, Vol. 40, 1966, pp. 1322–1330.

[9] Hegemier, G. A. and Morland, L. W.: "Stress Waves in a Temperature-Dependent Viscoelastic Half-Space Subjected to Impulsive Electromagnetic Radiation," *AIAA Journal*, Vol. 7, No. 1, Jan. 1969, pp. 35–41.

[10] Hegemier, G. A. and Tzung, F.: "Stress Wave Generation in a Temperature Dependent Absorbing Solid by Impulsive Electromagnetic Radiation," *Journal of Applied Mechanics*, June 1970, pp. 339–344.

[11] *Aviation Week*, Vol. 92, No. 2, Jan. 12, 1970; pp. 16–17; also *Physics Today*, Vol. 23, No. 7, July 1970, pp. 55–56.

[12] Penner, S. S., "Evaporation Coefficients From Exposure of a Solid to Laser Radiation," *AIAA Journal*, Vol. 2, No. 9, Sept. 1964, p. 1664.

[13] Timoshenko, S. P. and Goodier, J. N., *Theory of Elasticity*, McGraw-Hill, New York, 1951.

[14] "National Graphite Grade ATVS Technical Information Bulletin," No. 463-201-1G, Carbon Products Div., Union Carbide Corp., New York.

[15] Rhinehardt, J., private communication, Dec. 1969, Air Force Weapon-Lab. Albuquerque.
[16] Langmuir, I., "Chemical Reactions at Low Pressures," *Proceedings of the American Chemical Society*, 1915, p. 1139.
[17] Matting, F. W. and Chapman, D. R., "Analysis of Surface Albation of Noncharring Materials With Description of Associated Computing Program," TN-D-3758, 1966, NASA.
[18] Hirschfelder, J. O., Curtiss, C. F., and Bird, R. B., *Molecular Theory of Gases and Liquids*, Wiley, New York, 1954, p. 283.
[19] Altman, R. L., Unpublished Paper, 1970, NASA.
[20] Fogaroli, R. P. and Brant, D. N., "Re-Evaluation of Graphite Thermochemical Ablation," Fundamentals Memo TFM-9151-060, 1968, Thermodynamics Lab., General Electric.
[21] Dolton, T. A., Maurer, R. E., and Goldstein, H. E., "Thermodynamic Performance of Carbon in Hyperthermal Environment," AIAA Paper 68-754, Los Angeles, Calif., 1968.
[22] Schoessow, G. J., "Graphite Triple Point and Solidus-Liquidus Interface Experimentally Determined up to 1000 Atmospheres," CR-1148, 1968, NASA.
[23] Zavitsanos, P. D., "Experimental Study of the Sublimation of Graphite at High Temperatures," Final Report Contract AT(929-1)-789, 1969, Sandia Labs., Albuquerque.
[24] Boehringer, J. C. and Spindler, R. J., "Radiant Heating of Semi-Transparent Materials," *AIAA Journal*, Vol. 1, No. 1, Jan. 1963, p. 84.

OCTOBER 1971 AIAA JOURNAL VOL. 9, NO. 10

Asymptotic Solution for Viscous, Absorbing, Emitting Shock Layer

MARTIN C. JISCHKE*
University of Oklahoma, Norman, Okla.

Absorbing, emitting, high Reynolds number flow in the blunt body stagnation region is studied using asymptotic expansions. In contrast to previous results for optically thin gases, the boundary layer is here shown to be radiating and scale as $Re^{-1/2}$ with corrections of order (ln $Re)^{1+j}Re^{-1/2}$. Typical parameter values suggest the boundary layer to be weakly radiating. The primary effect of radiative transfer in the inviscid portion of the shock layer on the boundary-layer flow is given by the reduced value of the inviscid gas enthalpy at the wall. Numerical calculations of skin friction and total heat transfer including both radiation-induced coupling of the radiation and convective components and contributions of higher-order corrections indicate reduction of the skin friction and convective heat transfer due to radiative transfer. The results are used to determine conditions for which the radiative and convective components of heat transfer are equal.

Nomenclature

a_i = constants
A = reference area
B_ν = Planck function
$\bar{B}_\nu$ = nondimensional Planck function
c = speed of light
C_f = skin-friction coefficient
E_n = nth order exponential integral function
f = reduced stream function
F = reduced stream function in boundary layer
$\bar{F}$ = $\partial F/\partial\bar{\Gamma}$
h = enthalpy
H = boundary-layer enthalpy
$\bar{H}$ = $\partial H/\partial\bar{\Gamma}$
j = 0,1 for two-dimensional and axisymmetric flow, respectively
L = shock layer thickness scale
m = exponent in variation of density with enthalpy
N = $\rho\mu/\rho_s\mu_s$
p = pressure
Pr = Prandtl number
q^R = radiative heat flux
q^c = convective heat flux
r = radius from axis of symmetry
Re = Reynolds number
T = temperature
u,v = velocity components in the x and y directions, respectively
x,y = coordinates parallel to and normal to the body, respectively
y^* = value of y in overlap region
α = exponent in variation of temperature with enthalpy
β = exponent in variation of mass absorption coefficient with temperature
γ = Euler constant, 0.577...
Γ = radiation-convection energy parameter
$\bar{\Gamma}$ = boundary-layer radiation-convection energy parameter
δ_1,δ_2 = small parameters of boundary-layer expansion
ϵ_1 = small parameter of inviscid layer expansion
ζ = boundary-layer coordinate
η = normalized optical variable
$\bar{\eta}$ = boundary-layer optical variable
κ = mass absorption coefficient
κ_p = Planck mean mass absorption coefficient
μ = viscosity coefficient
ν = frequency
π^2 = pressure gradient parameter
ρ = density
σ = Stefan-Boltzmann constant
τ_L = shock layer optical depth
τ_s = reduced shock layer optical depth
τ_ν = optical depth at frequency ν
$\bar{\tau}_s$ = boundary-layer optical depth
φ_i = boundary-layer scaling parameters
ψ = stream function

Subscripts

ν = frequency dependent
w = wall
s = shock
0,1,2 = lowest, first, second order
thin = result obtained from optically thin analysis

Presented as Paper 70-868 at the AIAA 5th Thermophysics Conference, Los Angeles, Calif., June 29–July 1, 1970; submitted August 3, 1970; revision received March 22, 1971.

* Assistant Professor, School of Aerospace, Mechanical and Nuclear Engineering. Member AIAA.